ChemComm

COMMUNICATION

View Article Online
View Journal | View Issue

Cite this: *Chem. Commun.*, 2014, **50**, 11848

Received 15th July 2014,
Accepted 13th August 2014

DOI: 10.1039/c4cc05455e

www.rsc.org/chemcomm

High yield, controlled synthesis of graphitic networks from dense micro emulsions†

E. Negro,[a] M. Dieci,[b] D. Sordi,[b] K. Kowlgi,[b] M. Makkee[c] and G. J. M. Koper*[a]

We report on the production of Carbon Nano Networks (CNNs) from dense microemulsions in which catalyst nanoparticles have been synthesized. CNNs are 3D carbon networks, consisting of branches and junctions, and are mesoporous, graphitic, and conductive being suitable as electrode materials.

Amongst the allotropes of carbon, graphitic materials have the potential to foster advancements in nanotechnology as they possess a unique and remarkable combination of chemical, electronic, mechanical, optical, and thermal properties.[1–3] In most practical applications these special properties are, however, never suitably and fully utilized, as they are required over multiple directions and over large distances.[4–7] Cylindrical structures are mono-dimensional and in order to be applied in real life they have to become 2D/3D.[8] Therefore, it has been claimed that discrete particles of graphitic materials need to be connected to each other in order to deliver the required performance. The linkage of graphitic particles by covalent bonds addresses this issue, but only partially, as it is challenging if not impossible to create bonded structures with predetermined properties for two main reasons.[4–7] Firstly, the conventional production methods are only known to yield non-bonded graphitic particles such as Carbon Nano Tubes (CNTs).[9,10] Secondly, the current bonding techniques do not guarantee controllability or scalability of the inter-particle junctions.[4–7] Recent studies showed that it is possible to directly synthesize branched structures.[11–20] Low yields,[16,17] poor control over size and monodispersity,[11,12,17] necessity of a template[18] or specific process conditions, such as sulphur in the carbon source,[19,20]

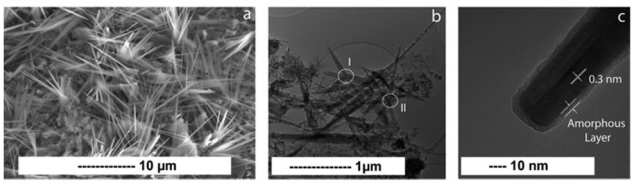

Fig. 1 CNNs imaged by (a) SEM showing branches and junctions, (b) TEM visualizing two junctions I and II, and (c) showing multiple walls with capped ends and a *d*-spacing of 0.3 nm. Around the branches a thin amorphous layer is visible.

were, however, reported and/or required. In this work, we propose a new hyper-branched carbon nano structure, called Carbon Nano Network (CNN), and its synthesis method which has the potential to alleviate these challenges as it grows directly into a networked structure of which the complexity can be tailored by experimental conditions to better suit its applications. These networks have a distinct morphology consisting of branches and junctions, Fig. 1a, with branches being the extended structures and junctions the places where branches converge: see circles in Fig. 1b and Fig. S1 and S2 (ESI†). The branches, Fig. 1c and Fig. S1 and S2 (ESI†), are composed of nanorods which are solid extended structures of concentric cylinders of graphene giving the appearance of a bundle.

Based on our experimental results and information available in the literature, the synthesis of CNNs can be described as a sequence of three phases of a single thermal chemical vapour decomposition process: the catalyst network formation phase, the growth phase, and the annealing phase; a sketch of the intermediate products is given in Fig. 2a. In the formation phase, phase 1 in Fig. 2b, the embedded catalyst consisting of metal nanoparticles (NPs), is networked into a carbon framework. In the growth phase, phase 2 in Fig. 2b, the catalyst decomposes ethene into 'carbon' at typically 700 °C thereby expanding the carbon framework by branched structures. In the annealing phase, phase 5 in Fig. 2b, at typically 1000 °C in an inert atmosphere, the crystallinity of the obtained 'carbon' structures is improved by transforming amorphous carbon and by removing side-products.

[a] *Section Advanced Self-Assembled Materials, Department of Chemical Engineering, Delft University of Technology, Julianalaan 136, 2628BL, Delft (NL), The Netherlands. E-mail: g.j.m.koper@tudelft.nl*
[b] *CarbonX, Julianalaan 136, 2628BL, Delft (NL), The Netherlands*
[c] *Section Catalysis Engineering, Department of Chemical Engineering, Delft University of Technology, Julianalaan 136, 2628BL, Delft (NL), The Netherlands*

† Electronic supplementary information (ESI) available. See DOI: 10.1039/c4cc05455e

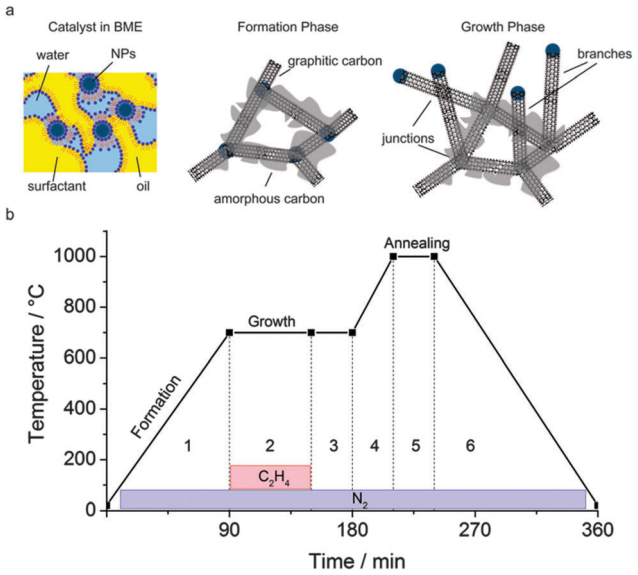

Fig. 2 (a) Sketch of catalyst NPs embedded in BMEs, formation phase and growth phase. (b) Heating profile. Ethene is sent to the reactor during the growth phase, otherwise the reactor is purged with nitrogen. In case annealing is not taking place after synthesis, the reactor is cooled down to room temperature after phase 3.

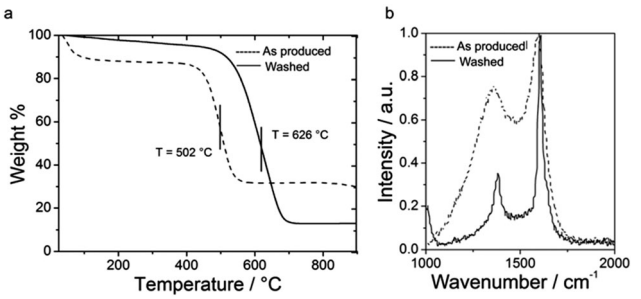

Fig. 3 (a) TGA profiles of decomposition in air, where the temperature of oxidation T corresponds to the temperature at which the derivative of the weight loss as a function of temperature presents a peak. (b) Raman spectrum for CNNs produced with the TX-system before and after acid washing.

The novelty of the present method lies in the formation phase where a carbon network is created between the high density catalyst NPs. Despite the high temperatures, this is not accompanied by significant NP agglomeration that would otherwise lead to a reduced catalytic activity. Previously proposed methods for catalyst stabilization involve dilute surfactant solutions[21] or a silica coating.[6] However, for the dilute surfactant solutions used, the NP synthesis methods are limited in yield. Higher yields are possible at the cost of NP aggregation that leads to a reduced activity. Alternatively, using a silica coating for the NPs involves an additional process step and moreover limits the attainable catalyst density. Here, in the present study, we produce NPs by dense bicontinuous microemulsions (BMEs) containing at least 50% of surfactant, Na-AOT or Triton X-100 (TX-100), by mass. BMEs have recently been demonstrated to be optimal for the high-yield production of monodisperse metal NPs.[22,23] Using this method, NPs of 2–4 nm with a narrow size distribution and coefficient of variation (CV) $\approx$ 20%, can be synthesized with an exceptionally high yield, up to 3% by synthesis mixture mass.[22] During the formation phase in an inert atmosphere, the temperature is slowly raised from ambient up to the reaction temperature, see the equivalent TGA-experiment profiles in Fig. S3a (ESI†). The product obtained after this phase results from the carbonization of the precursor fluid consisting of catalyst NPs such as Pt, Fe, Co, or Ni, embedded in a BME and loaded on a titanium, silicon, or carbon support, or without, into a crucible. After the evaporation of the volatile components, including the cracked hydrocarbons derived from the decomposition of the surfactant, the remainder is a rigid sponge-like structure that keeps the catalyst NPs well separated in their 3-dimensional arrangement, see Fig. S3b, c and S4 (ESI†). From the Raman spectroscopy, the carbon nanostructure obtained after the formation phase is found to be partially graphitic as observed by the presence of the G band, see Fig. S5 (ESI†). The NPs catalyze the formation of graphitic structures from the cracked hydrocarbons, being the primary carbon source. After the formation phase, the product, and thus the residuals of the TGA experiments differ significantly in composition for the different BMEs used, see Fig. S3a (ESI†). For Na-AOT-based BMEs, a residual of 8% in mass at 700 °C can be observed while for TX100 the residual is only 1% in mass. Besides the metal NPs, the residual consists of other hetero-atoms such as S and O or Na salts. For TX100 the residual mass is lower as it decomposes into more volatile components. However, after the growth and annealing phase, not the entire product turns out to be graphitic. This is illustrated in Fig. 3a and Fig. S6 (ESI†) that give the temperature of oxidation of CNNs before and after acid washing together with the residual mass after purification. The thermal resistance of the CNNs significantly rises after the purification because of the decomposition of amorphous or more defected carbon from the nanorod surface. Raman spectroscopy after washing, see Fig. 3b, shows a significant reduction, from 0.75 to 0.35, of the D/G-band intensity ratio, which is proportional to the amount of defects inside the graphitic structure, and a sharpening of the peaks, indicating a much higher level of order.[24] The acid washing also removes the inorganic material such as Na salts which leads to a lower residual mass.

We observed different types of junctions in CNNs depending on their origin. In Fig. 4a, rods are connected to the carbonized BME matrix with junctions inside the matrix. Here, the junction density is relatively high with small branches in between. The junctions constitute the nucleation points for the remaining structure consisting of carbon subsequently produced by ethene decomposition, Fig. 4b and c. Outside the carbonized matrix, the junctions are formed by crossing rods, Fig. 4b, or by merging rods, Fig. 4c, while the catalyst is found inside the carbon nanostructure, Fig. 4d, see also Fig. S1 and S2 (ESI†). The catalyst NPs are essential in catalysing the growth of carbon nanostructures while silicon and titanium serve as supports. As a matter of fact, without catalyst NPs the matrix does not result in CNNs, Fig. S7 (ESI†). From EDX mapping, Fig. 4e, it is clear that rods and networks are mainly composed of carbon. Metal NPs can be found at the tips or in the junctions. Sulphur is present but

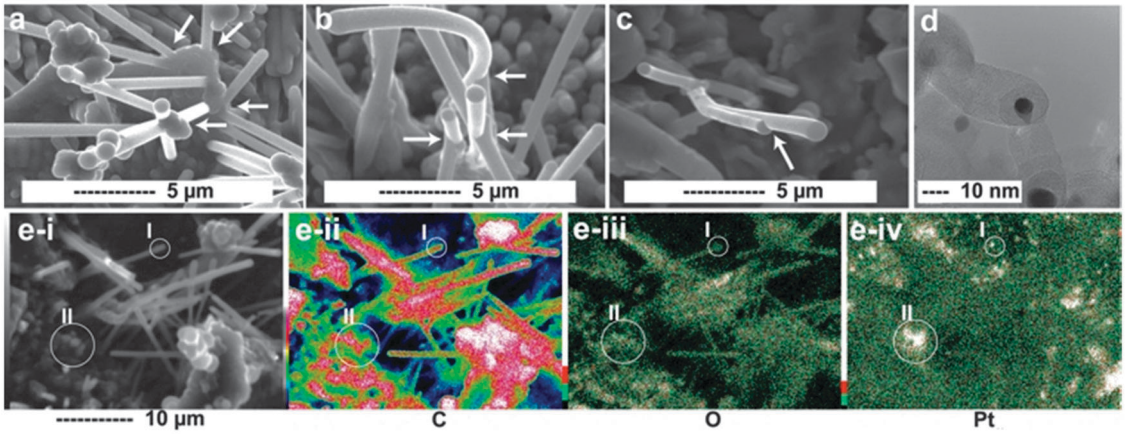

Fig. 4 SEM images of possible type of networks: (a) junctions originating from the BME matrix, (b) junctions from the crossing of two growing tubes, and from (c) merging rods. (d) TEM images of Pt NPs inside CNNs. (e-i) SEM image of CNNs produced from Pt NPs, with the annealing phase, and EDX mapping: (e-ii) carbon, (e-iii) oxygen, (e-iv) platinum, respectively.

not detectable. Table S1 (ESI†) reports the composition of the sample with Fig. S8 (ESI†) mapping the distribution of Si, Ti and Na. From EDX mapping it is evident that hetero-atoms, such as O, are present all over the structure, as confirmed by Raman spectroscopy measurement by the presence of the D band, Fig. S9a (ESI†). The D/G-band intensity ratio of CNNs as produced is however always below 1, usually 0.8 before annealing and 0.9 after annealing, Fig. S9b (ESI†).

The formation of CNNs involves the intricate interplay of nanorod growth and subsequent bundling into branches during the growth phase. The process conditions affect this interplay as summarized in Fig. S10 (ESI†). The reaction time has not been considered because it was assumed to be long enough to terminate nanostructure growth.[25] This interplay is expected to be minimal at a low catalyst density since rods can grow more extensively or even less unhindered.

The yield is high, up to 250 mg_{CNNs} mg_{metal}^{-1} which is as high as the maximum reported yield for CVD grown CNTs from metal NPs.[1] Uniform rods with a diameter of 0.7 ± 0.2 μm and a length of 54 ± 14 μm can be achieved, see Fig. S10b (ESI†). The size distributions are narrow, CV $\approx$ 29%. For higher catalyst concentrations, interactions between growing rods will become important and the formation process will be slowed down significantly leading to a lower CNN yield, Fig. S10a (ESI†). The slowing down of CNN formation with catalyst concentration also leads to thicker branches, up to diameters of 1.3 ± 0.4 μm, as more nanorods merge and hence also to shorter branches, 18 ± 7 μm, as the growth is more hindered, Fig. S10b (ESI†). The size distributions are slightly broader with CV $\approx$ 36%. Annealing, besides leading to purer CNNs, has a major impact on the size of the structures that become at least one order of magnitude bigger compared to that when no annealing is performed. CNN produced without annealing can have a diameter reduced to 0.1 ± 0.04 μm and length of 2.1 ± 1 μm, Fig. S10c (ESI†). Other factors, such as the reactor temperature and reactant feed, have a much smaller impact on geometrical properties: at most one order of magnitude, see Fig. S10c and d (ESI†). Results for CNNs grown from other metal catalysts, other BMEs and over various supports are presented in Fig. S11–S13 (ESI†), respectively. A similar dependence of process factors on the final structures was observed.

Various applications of CNNs have been investigated. Pilot experiments have shown that CNNs have a better ability to disperse than CNTs in polymers and polar solvents due to the presence of heteroatoms such as O in the structure, Fig. 4e, making them less hydrophobic.[26] The structure of CNNs can prove clearly advantageous where the interconnections are required such as needed for the electrically conductive catalyst supports. We synthesized CNNs directly over Carbon Paper (CP), see Fig. S13a (ESI†), and we measured the electrochemical response, see Fig. 5a. The capacitance increases 10 times compared to bare CP and no significant increase in ohmic resistance was observed. A quinone redox peak occurs at 0.6 V, indicating that the oxygen detected from EDX, Fig. 4e-iii, is partially located on the surface. This can be beneficial for catalytic applications.[27] Dielectric spectroscopy shows CNNs to be well conductive, see Fig. S14 (ESI†). Additionally, BET measurements, see Fig. 5b, show that CNNs have a high surface area, 110 m^2 g^{-1}, and are mainly mesoporous, see Fig. 5c. Finally, the 3D nature and better wettability of CNNs make them potentially less nano-toxic than CNTs, whose mono-dimensionality and hydrophobicity

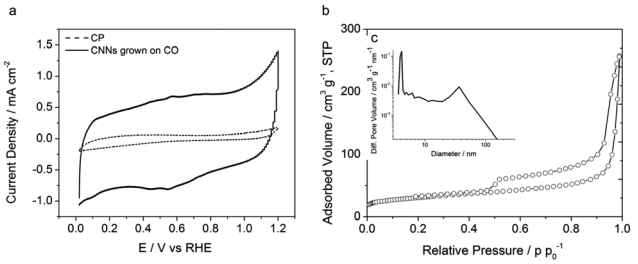

Fig. 5 (a) Cyclic voltammetry performed in 0.5 M H_2SO_4, N_2 saturated, scan rate 20 mV s^{-1}, of bare Carbon Paper (CP) and CNNs grown from Fe and TX100 on CP. (b) BET measurement of CNNs. (c) Pore size distribution from BET measurements.

have been addressed as the reasons for deep penetration in the human body and low biocompatibility.[28,29] These properties and their high chemical stability in an oxidizing environment as shown in Fig. 3a make CNNs promising materials for electrocatalytic applications, for example in polymer electrolyte membrane fuel cells.[30,31]

To summarize, we have presented a high yield, versatile synthesis of highly connected graphitic carbon nanostructures catalysed by metal NPs synthesized in BMEs. No inorganic support is necessary to synthesize these networks that are three-dimensional with controllable size. CNNs are graphitic, mesoporous, and conductive and are promising for, as an example, catalytic applications or as electroconductive materials. Clearly, the here presented CNNs can replace bonded CNTs in most applications because they grow directly into a networked structure having isotropic properties.

We thank Dr Patricia Kooyman for TEM micrographs, Ing. Harrie Jansma for help with the experimental setup, Piet Droppert for dielectric spectroscopy measurements, Prof. Stephen Picken, Prof. Dr Jan H. van Esch, Dr Rienk Eelkema, Dr Simge Tarkuc and Dr Dainius Janeliunas for discussions. We acknowledge financial support from the Advanced Dutch Energy (ADEM) Program.

Notes and references

1 L. Mleczko and G. Lolli, *Angew. Chem., Int. Ed.*, 2013, **52**, 9372–9387.
2 Q. Zhang, J.-Q. Huang, W.-Z. Qian, Y.-Y. Zhang and F. Wei, *Small*, 2013, **9**, 1237–1265.
3 Y. Shen, L. Yan, H. Song, J. Yang, G. Yang, X. Chen, J. Zhou, Z.-Z. Yu and S. Yang, *Angew. Chem., Int. Ed.*, 2012, **51**, 12202–12205.
4 D. Wei and Y. Liu, *Adv. Mater.*, 2008, **20**, 2815–2841.
5 M. Meyyappan, *J. Phys. D: Appl. Phys.*, 2009, **42**, 213001.
6 S. Takenaka, T. Iguchi, E. Tanabe, H. Matsune and M. Kishida, *Carbon*, 2009, **47**, 1251–1257.
7 G. S. Roberts and P. Singjai, *Nanoscale*, 2011, **3**, 4503–4514.
8 A.-H. Lu, G.-P. Hao and Q. Sun, *Angew. Chem., Int. Ed.*, 2013, **52**, 7930–7932.
9 M. J. Behr, K. A. Mkhoyan and E. S. Aydil, *ACS Nano*, 2010, **4**, 5087–5094.
10 O. V. Yazyev and A. Pasquarello, *Phys. Status Solidi B*, 2008, **245**, 2185–2188.
11 G. K. Goswami, R. Nandan and K. K. Nanda, *Carbon*, 2013, **56**, 97–102.
12 Z. He, J.-L. Maurice, C. Seok Lee, C. S. Cojocaru and D. Pribat, *CrystEngComm*, 2014, **16**, 2990–2995.
13 S. Huang, L. Dai and A. Mau, *Phys. B*, 2002, **323**, 336–338.
14 G. Meng, Y. J. Jung, A. Cao, R. Vajtai and P. M. Ajayan, *Proc. Natl. Acad. Sci. U. S. A.*, 2005, **102**, 7074–7078.
15 X. Tao, X. Zhang, J. Cheng, Y. Wang, F. Liu and Z. Luo, *Chem. Phys. Lett.*, 2005, **409**, 89–92.
16 D. C. Wei, L. C. Cao, L. Fu, X. L. Li, Y. Wang, G. Yu and Y. Q. Liu, *Adv. Mater.*, 2007, **19**, 386–390.
17 J. F. AuBuchon, L.-H. Chen, C. Daraio and S. Jin, *Nano Lett.*, 2006, **6**, 324–328.
18 Y. Fu, B. Carlberg, N. Lindahl, N. Lindvall, J. Bielecki, A. Matic, Y. Song, Z. Hu, Z. Lai, L. Ye, J. Sun, Y. Zhang, Y. Zhang and J. Liu, *Adv. Mater.*, 2012, **24**, 1576–1581.
19 G. H. Du, W. Z. Li, Y. Q. Liu, Y. Ding and Z. L. Wang, *J. Phys. Chem. C*, 2007, **111**, 14293–14298.
20 W. Z. Li, B. Pandey and Y. Q. Liu, *J. Phys. Chem. B*, 2006, **110**, 23694–23700.
21 M. F. Sarac, R. M. Wilson, A. C. Johnston-Peck, J. Wang, R. Pearce, K. L. Klein, A. V. Melechko and J. B. Tracy, *ACS Appl. Mater. Interfaces*, 2011, **3**, 936–940.
22 K. Kowlgi, U. Lafont, M. Rappolt and G. Koper, *J. Colloid Interface Sci.*, 2012, **372**, 16–23.
23 E. Negro, R. Latsuzbaia and G. Koper, *Langmuir*, 2014, **30**, 8300–8307.
24 F. Jaouen, A. M. Serventi, M. Lefèvre, J.-P. Dodelet and P. Bertrand, *J. Phys. Chem. C*, 2007, **111**, 5971–5976.
25 V. Jourdain and C. Bichara, *Carbon*, 2013, **58**, 2–39.
26 K. N. K. Kowlgi, G. J. M. Koper and R. A. D. Van Raalten, WO2012036555, Delft Enterprises B.V., 2012.
27 A. Sarapuu, K. Helstein, K. Vaik, D. J. Schiffrin and K. Tammeveski, *Electrochim. Acta*, 2010, **55**, 6376–6382.
28 L. Yan, F. Zhao, S. Li, Z. Hu and Y. Zhao, *Nanoscale*, 2011, **3**, 362–382.
29 K. Kostarelos, *Nat. Biotechnol.*, 2008, **26**, 774–776.
30 E. Negro, M. A. D. Vries, R. Latsuzbaia and G. J. M. Koper, *Fuel Cells*, 2014, **3**, 350–356.
31 P. Yu, W. Gu, J. Zhang, R. Makharia, F. Wagner and H. Gasteiger, in *Polymer Electrolyte Fuel Cell Durability*, ed. F. Büchi, M. Inaba and T. Schmidt, Springer, New York, 2009, pp. 29–53.